

ROTOR POWER REDUCTION USING MULTIPLE SPANWISE-SEGMENTED, OPTIMALLY-ACTUATED TRAILING-EDGE FLAPS

Olivier Léon[†] Farhan Gandhi[‡]

Vertical Lift Research Center of Excellence (VLRCOE)
Department of Aerospace Engineering
The Pennsylvania State University
University Park, Pennsylvania, USA

ABSTRACT

Spanwise-segmented Trailing Edge Flaps (TEFs) were examined for rotorcraft power reduction. Four TEFs, extending from 50-60%, 60-70%, 70-80% and 80-90% span, were considered and actuated at frequencies up to 2/rev. A gradient-based optimization scheme was used to determine the optimal deployment of the TEFs that minimized rotor power, while satisfying vehicle trim. Studies were based on a UH-60 type aircraft and the effect of the TEFs was examined at moderate to very high speeds, and for low through high aircraft gross-weights. In the analysis CFD generated lift and drag increments associated with TEF deflections were added to airfoil properties of the base SC-1094R8 airfoil. At high gross-weight and airspeed, reductions in rotor power of up to nearly 8% were observed for blades with a -8 deg linear twist, and up to 5.65% when the nonlinear twist of the UH-60 was used. The power reduction was predominantly due to a reduction in profile power, especially at the higher gross weights and advance ratios. In general, the TEFs moved lift inboard and offloaded the tip regions. Even though the drag increased slightly inboard, the large reduction in drag along the outer rim, along with the large moment arm, reduced rotor torque and power.

NOTATION

dD	Sectional drag
dL	Sectional lift
N_b	Number of blades
P_0	Rotor profile power
P_i	Rotor induced power
P_p	Rotor propulsive power
r	Radial location
TEF	Trailing Edge Flap
δ	TEF deflection angle (positive down)
θ	Blade pitch angle
μ	Rotor advance ratio
φ	Inflow angle
Ψ	Azimuth angle
Ω	Rotor angular velocity

1. INTRODUCTION

Over the last couple of decades tremendous effort has been devoted to the area of rotor vibration reduction using active control technologies (see, for example, Ref. [1] which provides a comprehensive survey of such efforts). The technologies considered have included

Higher Harmonic blade pitch Control (HHC) implemented through the swashplate as well as Individual Blade Control (IBC) implemented either at the blade root via active pitch links, through active twist of the rotor blades or by way of trailing-edge flaps. Computational studies, wind-tunnel tests as well as flight-tests have all shown that rotor vibrations can be reduced very significantly using inputs primarily at $(N-1)/rev$, N/rev and $(N+1)/rev$, for an N -bladed rotor. Efforts, although not quite as extensive, have also been devoted to examining potential reductions in rotor power requirement through the use of rotor active control. Reducing rotor power requirement can increase the endurance, range, and payload capabilities of the aircraft.

The first active control technology that was considered for rotor power reduction was HHC, but its effect remains inconclusive. Some studies report negligible reduction (Refs. [2-5]) or even increase (Refs. [6-8]) in power, while a couple of studies have reported power reduction (Refs. [9], [10]). In Ref. [9], Shaw et al. conducted a wind-tunnel test on a model 3-bladed articulated CH-47D rotor and observed power reductions of 6% at 135 kts and 4% at 160 kts using 2/rev inputs of 2 deg amplitude. In Ref. [10], Nguyen and Chopra examined power reductions on the same model CH-47D rotor tested in Ref. [9], using a comprehensive analysis. Up to 3.8% power reduction was reported at high speeds using 2 deg, 2/rev inputs, but this was accompanied by a large increase in 2/rev in-plane blade root shear loads. The power reductions reported in Refs. [9] and [10] do not account for actuation power requirements.

Jacklin et al. (Refs. [11], [12]) examined the effect of 2/rev root pitch IBC for reducing the power of a full-scale

[†]Graduate Research Assistant

[‡]Professor, fgandhi@engr.psu.edu

35th European Rotorcraft Forum, Hamburg, Germany.
September 22-25, 2009.

BO-105 (4-bladed, hingeless) rotor in the 40x80 wind-tunnel at NASA Ames Research Center. At moderate speeds no power reductions were measured, but at high speeds ($\mu=0.4$) power reductions of 4% with 1 deg IBC amplitude and up to 7% with 2 deg IBC amplitude were reported. However, the authors noted that when actuation power is considered, the net gains are substantially reduced (to approximately 2.5%). In Ref. [13] Cheng et al. computationally examined the power reductions possible on a UH-60 type 4-bladed articulated helicopter using 2/rev root pitch IBC inputs. For a properly phased 2/rev input of amplitude 1 deg, power reductions of up to 1.5% for moderate gross weight and up to 3.8% for high gross weight were reported. These results were obtained using a simplified structural model and a linear inflow model. In Ref. [14], however, the power reductions on the same configuration were significantly reduced (to the point of being virtually eliminated) when a free-wake model was used to represent the inflow around the rotor disk. Recently, the effect of 2/rev root pitch IBC input on power reduction of a CH-53G was measured in a flight-test (Refs. [15], [16]). An IBC amplitude of 0.67 deg, with proper phasing, resulted in a measured torque reduction of 2% at 130 kts. However, the authors estimate that the net rotor power reduction after correction for trim would be of the order of 6%.

The effect of using trailing-edge flaps for power reduction on a BO-105 type 4-bladed hingeless rotor helicopter was examined, computationally, by Liu et al. (Ref. [17]). Unlike the previous root-pitch IBC studies which focused on 2/rev inputs, 2-5/rev inputs of the trailing-edge flap were used. At an advance ratio of 0.35 and moderate thrust, power reductions of 1.73% (single flap) to 1.76% (dual flaps) were reported, but the vibrations were increased by 100%. When the objective function considered both power and vibrations, the power reductions obtained were limited to 0.67% with dual flaps. Although slightly larger power reductions were obtained using a nonlinear algorithm, this algorithm could not be implemented in real-time due to the high computational cost. Larger power reductions of up to 1.46% were reported at higher thrust levels, increasing to 1.82% at very high thrust levels. Increasing the advance ratio to 0.4 resulted in possible power reductions of up to 4.04%. The reported flap deflection requirements were generally under 3 deg. An accurate assessment of the power reductions requires high-fidelity modeling of the trailing-edge flap drag. However, the drag was modeled very simplistically in their study (assumed to vary linearly with the magnitude of the flap deflection, without considering any dependence on the airfoil angle of attack or the Mach number).

In Ref. [18], Yeo compared a variety of active control methods for helicopter performance improvement. The methods considered include leading edge slat, variable droop leading edge, oscillatory jet, Gurney flap, IBC, active twist and trailing edge flaps. An AH-64 Apache rotor system with blades incorporating VR-12 airfoil characteristics was considered. The effects of the active control technologies was added as increments in lift, drag and pitching moment to the VR-12 airfoil tables and the performance analysis was conducted using CAMRAD-II. The conclusions drawn from this study were that using IBC, active twist and TEF concepts can improve the rotor lift-to-drag ratio with a 2/rev harmonic control, and leading edge slat, variable droop leading edge, oscillatory jet and Gurney flap concepts can increase the maximum blade

loading when used over the retreating side of the rotor.

While one approach has been to use established active control methods to reduce rotor power (as seen in Refs. [2-17]), another different approach has been to calculate the optimal airload distribution that would minimize rotor power (while meeting other trim targets). In Ref. [19] Moffitt and Bissell calculated the optimum airload distribution for a UH-60 Black Hawk helicopter for minimum main rotor induced plus profile power. The optimal twist in hover was fairly similar to that of the Black Hawk, but power reductions of up to 10% were achievable at high speeds of 175 kts. Hall et al in Ref. [20] optimized the lift distribution corresponding to the minimum rotor induced power. At an advance ratio of 0.25 their results suggest possible reductions of 10%-15% in induced power requirement. A similar study was conducted by Rand et al. in Ref. [21]. They calculated the optimal azimuthal and spanwise circulation distribution using both prescribed as well as free-vortex wake models, and like Hall et al., obtained induced power reductions of up to 10% at advance ratios below 0.25. While these studies indicate that higher harmonic variation in airloads is generally required to realize the predicted power reductions, it is unclear how the required variation could be achieved. Indeed, this presents a significant challenge.

One of the limitations with using established active control methods for rotor power reduction is that while they allow for modification of airloads around the azimuth, they do not allow a simultaneous, independent tailoring of the airloads along the span. The studies that calculate optimal loads (such as Refs. [19-21]) do not have this constraint, so they generally predict larger power reductions. In Ref. [22], Bae et al. used *multiple, spanwise-segmented* Gurney flaps (4 flaps, each 10% span, extending over 50-90% of the blade radius, deployed at a combination of 1/rev and 2/rev), which provided some ability to optimally redistribute the airloads around the azimuth and along the span, simultaneously. The greater flexibility in redistributing the airloads yielded power reductions of up to nearly 9% for a UH-60 type rotor at high gross-weights and advance ratios. The power reductions are larger than those achieved using established active control methods that do not facilitate independent spanwise tailoring of airloads, and approach levels associated with optimal rotor disk airload distribution. However, a key distinction from the efforts in Refs. [19-21] was that these reductions could actually be realized using the spanwise-segmented Gurney flaps.

The present work is similar to the study reported by Bae et al. (Ref. [22]), but multiple spanwise-segmented Trailing-Edge Flaps (TEFs) are used to optimally redistribute the airloads, both radially and azimuthally, and minimize the rotor power requirement. TEFs are attractive because of low actuation force/power requirement (compared to HHC, root pitch IBC, or active blade twist), and can, in many conditions, have lower drag penalty (per unit increment in lift) compared to Gurney flaps (Ref. [23]). The study is based on UH-60A type helicopter with four TEFs, each 20% chord, 10% span, extending over 50-90% blade radius, as shown in Fig. 1. The objective of the study is to assess the potential of these spanwise-segmented TEFs actuated up to 2/rev, for total power reduction over a range of airspeeds and thrust levels, and understand the mechanisms through which power reduction is achieved.

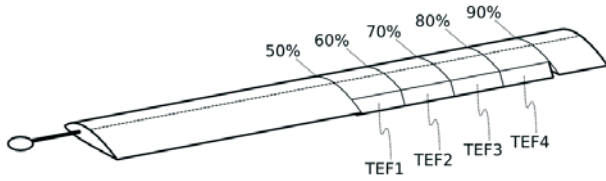


Figure 1. Multiple spanwise-segmented trailing edge flaps on a rotor blade.

2. ANALYSIS

In the present study simulations are conducted on an aircraft based on the UH-60A Black Hawk helicopter (key properties given in Table A1 in the Appendix). However, two different blade twist profiles are considered. The first is a -8 deg linear twist (many modern rotors have a linear twist in the range of -6 to -12 deg) and the second is the UH-60's actual nonlinear twist, depicted in Fig. A1 in the Appendix. The actual UH-60 blades use SC-1094R8 airfoils over 47–85% span, and SC-1095 airfoils elsewhere. However, in the present study the SC-1094R8 airfoil is extended up to 90% span (since the outermost TEF extends from 80–90% span, as discussed in the next paragraph). C81 tables for the SC-1095 and SC-1094R8 airfoils (from Ref. [28]) are used to obtain the sectional aerodynamic loads based on angle of attack and Mach number. The blades are modeled as undergoing rigid flap rotations about the offset flapping hinge but lag and torsion deformation is neglected in the analysis. This same simulation model (with the nonlinear twist of the UH-60A, and the proper airfoil distribution) has been used by Steiner et al. (Ref. [24]) and Bluman and Gandhi (Ref. [25]), and the trim parameters and rotor power predictions shows very good correlation with flight-test data as well as CAMRAD-II analysis results (see rotor power predictions in Fig. 2). Such a rigid-blade analysis with a good aerodynamic model is quite appropriate for trim and power predictions and becomes an excellent choice when coupling with an optimizer to determine the optimal TEF deflections for power minimization. Since the study does not focus on loads and vibrations, modeling elastic deformations of the blades is not critical. In fact, Cheng and Celi (Ref. [14]) showed that even if the baseline power levels predicted using rigid versus elastic blade models deferred slightly, the power reductions predicted using IBC as well as the optimal actuation phase required was the same, for both the rigid and elastic blade models.

Each blade is assumed to have 4 TEFs, each 10% span, extending from 50–60%, 60–70%, 70–80% and 80–90% span, as depicted in Fig. 1. The effects of the TEFs are modeled by adding increments in lift and drag coefficient to the baseline C81 airfoil tables. The aerodynamic coefficients of an SC-1094R8 airfoil with 20% chord TEF (Fig. 3) were computed in Refs. [26] and [27] over a large range of angles of attack, Mach numbers and TEF deflection angles using a 2D Navier-Stokes CFD code (OVERTURNS) configured for airfoils with TEFs.

The aerodynamic model includes a lifting line vortex wake model with prescribed geometry. The wake-induced velocity at the aerodynamic integration points along the blade span are calculated by using the Biot-Savart law, accounting for the contribution of each vortical element.

As an individual TEF deploys, the lift changes locally. This causes the strength of the bound vorticity as well as the trailed vorticity (especially at the edges of that TEF) to change which, in turn, changes the inflow distribution. Accounting for the change in vortex strength and inflow due to TEF deployment allows for an accurate calculation of the induced power. Cheng and Celi (Ref. [14]) showed that a vortex-wake method was important in calculating the power reductions associated with rotor active control. Since the current study focuses on power reductions at moderate to high cruise speeds ($\mu=0.3, 0.35$ and 0.4), the self-induced distortions in wake geometry, prominent at low speeds, are less important and a prescribed wake is considered sufficient. This is especially true in view of the fact that the analysis is coupled with an optimization scheme, requiring a good balance between computational cost and modeling fidelity.

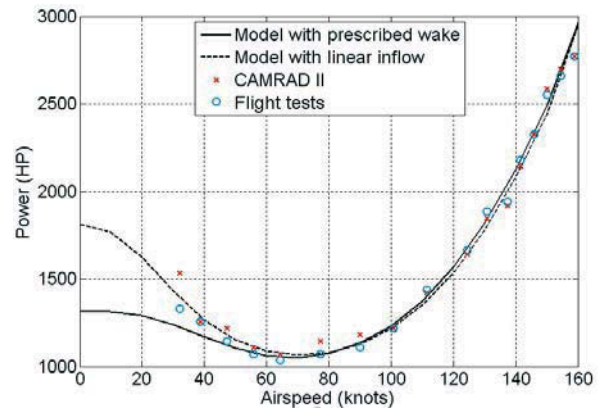


Figure 2. Total rotor power (HP) versus airspeed for UH-60A helicopter, 18,300 lbs gross weight.

The TEFs are each actuated up to 2/rev. Thus there are 5 input variables to define the deflection of each TEF: the steady deflection, δ_0 , the first harmonics δ_{1c} and δ_{1s} and the second harmonics δ_{2c} and δ_{2s} . The deflection of the TEF 'N' is then defined as:

$$\delta_N = \delta_0^{(N)} + \delta_{1c}^{(N)} \cos \psi + \delta_{1s}^{(N)} \sin \psi + \delta_{2c}^{(N)} \cos 2\psi + \delta_{2s}^{(N)} \sin 2\psi$$

The maximum deflection of any TEF is limited to 5 deg, so

$$\max |\delta_N| \leq 5^\circ$$

Considering the steady, 1/rev and 2/rev inputs of each of the 4 TEFs results in a total of 20 parameters or "design variables" that the optimizer determines while attempting to minimize the main rotor power.

$$\begin{cases} \text{minimize } P(\{\delta\}_{20 \times 1}) \\ \text{with } \{\delta\}_{20 \times 1} = [\delta_0^{(1)}, \delta_{1c}^{(1)}, \delta_{1s}^{(1)}, \delta_{2c}^{(1)}, \delta_{2s}^{(1)}, \dots, \delta_0^{(4)}, \delta_{1c}^{(4)}, \delta_{1s}^{(4)}, \delta_{2c}^{(4)}, \delta_{2s}^{(4)}] \\ \text{such that } \forall N \in [1 : 4] \max |\delta_N| \leq 5^\circ \end{cases}$$

The optimizer used in this study is MATLAB's gradient-based optimizer FMINCON. The optimization procedure requires that the aircraft remain in propulsive trim (constraint condition). In the implementation, the helicopter is simply re-trimmed in every iteration of the power minimization process. For each TEF a 2 deg steady deflection was used as an initial guess for the optimization process. Thus there is no guarantee that a global minima is achieved, and the solution in general

represents a local minima.

The present study accounts for the increment in lift and drag associated with the deployment of the TEFs, but not the pitching moment, since the rotor is modeled as torsionally rigid. It should be noted however, that unlike vibration reduction applications where the active control is generally at higher frequency, $(N-1)/rev$, N/rev and $(N+1)/rev$, and the elastic torsion mode is likely to be excited, in the current study the excitation is at lower frequencies (up to $2/rev$), so the elastic torsion mode is much less likely to be excited, especially if the rotor is torsionally rigid (frequencies of $\sim 5/rev$ and greater).



Figure 3. SC-1094R8 airfoil with 20% chord TEF.

In order to better understand the origins of the power reductions observed in the Results section, the total rotor power is decomposed into its constituents: induced power P_i , profile power P_0 and propulsive power P_p . Thus,

$$P_{total} = P_i + P_p + P_0$$

The total average power is calculated through integration of the rotor in-plane forces times the moment arm

$$P_{total} = \Omega \frac{N_b}{2\pi} \int \int (dL \cdot \sin(\varphi) + dD \cdot \cos(\varphi)) r d\psi$$

where dL and dD the sectional lift and profile drag forces and φ is the inflow angle. From the above equation, the second term on the right hand side is the profile power necessary to overcome viscous forces. Thus,

$$P_0 = \Omega \frac{N_b}{2\pi} \int \int (dD \cdot \cos(\varphi)) r d\psi$$

The first term on the right hand side of the expression for P_{total} is the sum of the induced plus propulsive power.

$$P_i + P_p = \Omega \frac{N_b}{2\pi} \int \int (dL \cdot \sin(\varphi)) r d\psi$$

The induced power, which represents the energy in the wake in order to produce lift, can be calculated directly as:

$$P_i = \int v_i dF_z$$

where v_i is the induced velocity across the rotor disk. However, in practice it is easier to calculate the propulsive power required to move the helicopter forward at an airspeed, V , as

$$P_p = F_{prop} \cdot V$$

And then calculate the induced power as

$$P_i = \left(\Omega \frac{N_b}{2\pi} \int \int (\sin \varphi dL) r d\psi \right) - (F_{prop} \cdot V)$$

F_{prop} is the resultant rotor force in the direction of V .

3. RESULTS

This section presents the power reductions obtained using optimal TEF deployments over a range of advance ratios and vehicle gross weights, for the -8 deg linear twist as well as the nonlinear twist cases. The optimal TEF deflections, their effect on redistribution of airloads around the rotor disk, and the mechanisms of yielding the power reductions are all discussed in detail.

3.1. Power Reductions with -8 deg Linear Twist

For the -8 deg linear twist case, optimal TEF inputs for power reduction were calculated for advance ratios of 0.3, 0.35 and gross weights of 16,000 lbs, 18,300 lbs and 22,000 lbs, and also for an advance ratio of 0.4 and gross weight of 16,000 lbs. Optimal TEF schedules for $\mu = 0.4$, 18,300 lbs and 22,000 lbs gross weight, could not be obtained due to convergence problems in the optimization process.

Table 1 summarizes the power reductions obtained for different conditions. These are presented both in terms of percent power reductions (Table 1a) and actual reductions in horsepower (Table 1b). Power reductions of 7-8% are observed for high gross weights or advance ratios, while reduction of 4.3% is observed at low gross weight and moderate advance ratio. Table 2 summarizes the actual power requirements of the baseline and the optimally flapped rotor for each flight condition.

In order to understand the source of the power reductions, reductions in profile power and induced power are individually examined in Tables 3 and 4, respectively. These are once again presented in terms of percent reductions (Table 3a and 4a) and actual reductions in horsepower (Table 3b and 4b). Comparing Tables 3b and 4b, it is clear that in all the cases considered the reduction in profile power is significantly greater than that in induced power. At higher advance ratios and gross weights, the profile power reduction dominates induced power reduction to an even greater extent. For 16,000 lbs gross weight, at $\mu = 0.3$, reductions in profile and induced power are 46.51 HP and 27.33 HP, respectively; but at $\mu = 0.4$, corresponding reductions in profile and induced power are 221.33 HP and 57.85 HP, respectively. This seems reasonable since induced power becomes less significant at higher advance ratios, so reductions in power are obtained primarily through reductions in profile power.

The optimal TEF deflections result in a reduction of rotor collective pitch, as seen in Table 5. A decrease in collective pitch, θ_0 , of 0.9 deg to 1.2 deg is observed, but the cyclic controls, θ_{1c} and θ_{1s} , do not show a significant change. The reduction in collective pitch is expected to reduce the angles of attack across the rotor disk with a corresponding reduction in lift and drag while the TEFs provide an increment in lift in the regions where they are deflected. In order to gain a better understanding, a more detailed examination of the rotor forces and aerodynamic environment is carried out in the following sections. Two cases are discussed in detail: $\mu = 0.3$, 18,300 lbs gross weight; and $\mu = 0.35$, 22,000 lbs gross weight.

3.2. Analysis, $\mu = 0.3$, 18,300 lbs Gross Weight

At an advance ratio of 0.3 and a gross weight of 18,300 lbs, a total power reduction of 5.53% was observed (Table 1). The optimal TEF deflections that resulted in this power reduction are shown in Fig. 4. The deflections of

Table 1. Total power reduction: (a) percent, and (b) difference in HP, at different advance ratios and gross weights (lbs), -8 deg linear twist.

(a)			
	0.3	0.35	0.4
16,000	4.3	5.7	7.35
18,300	5.53	6.57	N/A
22,000	7.5	7.98	N/A

(b)			
	0.3	0.35	0.4
16,000	73.84	142.54	279.18
18,300	101.84	173.47	N/A
22,000	158.11	236.8	N/A

Table 2. Total power requirement (HP) for baseline and optimal TEF cases, -8 deg linear twist.

		Advance ratio			
		0.3	0.35	0.4	
Gross weight	16,000	1715.61	2498.73	3797.27	Baseline
		1641.77	2356.18	3518.09	Optimal
	18,300	1841.97	2640.81	3968.18	Baseline
		1740.12	2467.34	N/A	Optimal
	22,000	2107.90	2966.83	4608.16	Baseline
		1949.79	2730.02	N/A	Optimal

Table 3. Profile power reduction: (a) percent, and (b) difference in HP, at different advance ratios and gross weights (lbs), -8 deg linear twist.

(a)			
	0.3	0.35	0.4
16,000	8.33	13.93	19.3
18,300	11.82	16.24	N/A
22,000	16.74	19.21	N/A

(b)			
	0.3	0.35	0.4
16,000	46.51	105.75	221.33
18,300	70.44	131.6	N/A
22,000	117.47	190.01	N/A

Table 4. Induced power reduction: (a) percent, and (b) difference in HP, at different advance ratios and gross weights (lbs), -8 deg linear twist

(a)			
	0.3	0.35	0.4
16,000	5.8	5.86	6.18
18,300	5.2	5.75	N/A
22,000	5.17	4.75	N/A

(b)			
	0.3	0.35	0.4
16,000	27.33	36.79	57.85
18,300	31.4	41.87	N/A
22,000	40.64	46.79	N/A

Table 5. Rotor pitch controls for baseline and optimal TEF cases, -8 deg linear twist.

	θ_0		θ_{1c}		θ_{1s}	
	Baseline	Optimal	Baseline	Optimal	Baseline	Optimal
$\mu = 0.3, W = 16k$ lbs	5.784	4.812	2.787	2.466	-7.803	-7.358
$\mu = 0.3, W = 18.3k$ lbs	6.099	4.953	2.948	2.622	-7.719	-7.334
$\mu = 0.3, W = 22k$ lbs	6.830	5.631	3.248	3.022	-7.903	-7.627
$\mu = 0.35, W = 16k$ lbs	8.202	7.078	3.392	2.925	-10.284	-9.880
$\mu = 0.35, W = 18.3k$ lbs	8.343	7.181	3.548	3.218	-9.928	-9.543
$\mu = 0.35, W = 22k$ lbs	8.937	7.802	3.870	3.704	-9.863	-9.541
$\mu = 0.4, W = 16k$ lbs	11.654	10.480	4.265	3.747	-12.963	-12.780

each of the TEFs comprise of a combination of steady, 1/rev and 2/rev components such that the deflections are larger on the entire retreating side of the rotor disk and smaller on the advancing side. Large deflections on the retreating side increase the effective camber in that region; whereas the smaller deflections on the advancing side, especially for the outboard TEFs, can be related to the drag penalty associated with TEF deployment at high Mach numbers. The values of the optimal steady, 1/rev, and 2/rev TEF deflections for this case (as well as for the other cases) are presented in Table A2 in the Appendix. From Fig. 4 it is observed that the TEF deflection is never negative (no upward deflection), so the TEFs are only adding lift, after reduction in rotor collective has reduced lift elsewhere.

Figures 5a and 5b show the lift distribution around the rotor disk with optimal TEF deployments and for the baseline rotor, respectively, while Fig. 5c shows the difference between the two. From Fig. 5c it is observed that the TEFs increase the lift inboard (over 50-90% span), while offloading the tips (due to reduction in rotor collective pitch). The largest increases in lift appear to be on the advancing side and the front and the rear of the rotor disk. Even though the flap deflections are largest on the retreating side, smaller deflections on the advancing side along with the high Mach numbers are seen to be very effective in increasing the inboard lift on the advancing side.

Similarly, Figs. 6a and 6b show the drag distribution around the rotor disk with optimal TEF deployments and for the baseline rotor, respectively, while Fig. 6c shows the difference between the two. For the baseline rotor, the drag is highest near the tip in the fourth quadrant, particularly at the rear of the rotor disk (Fig. 6b). The TEFs, by unloading the tips, reduce the drag along the outer rim (Fig. 6c), but the drag generally increases

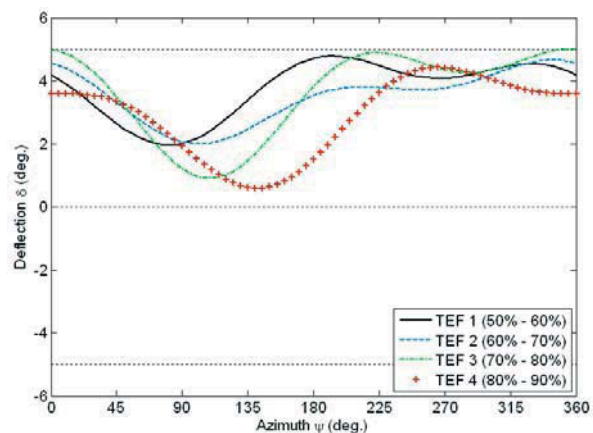


Figure 4. Optimal TEFs deflections; -8 deg linear twist, $\mu = 0.3$, 18,300 lbs gross weight.

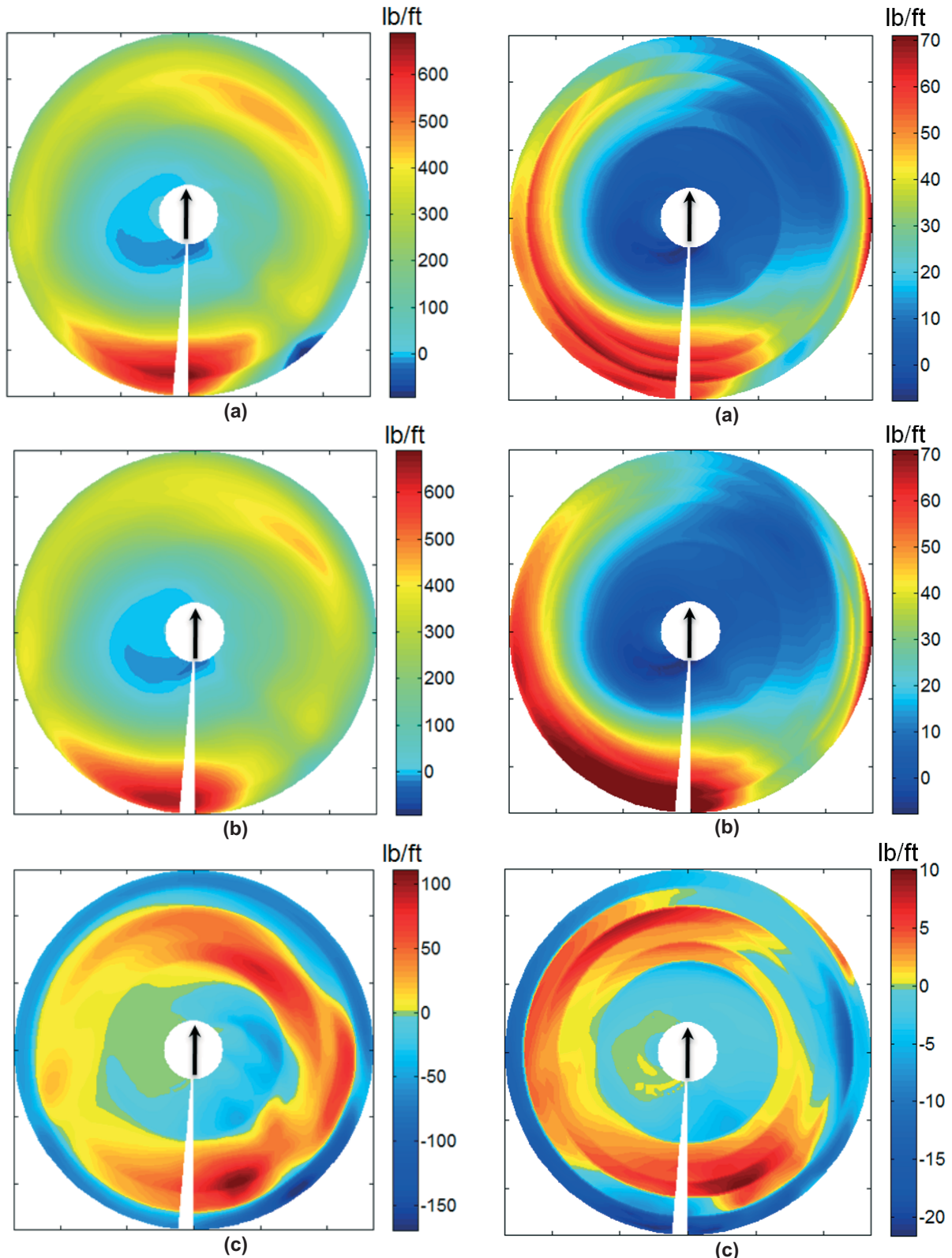


Figure 5. Lift distribution (a) with optimal TEF deployment, (b) baseline, and (c) difference between a and b; -8 deg linear twist, $\mu = 0.3$, 18,300 lbs gross weight.

Figure 6. Drag distribution (a) with optimal TEF deployment, (b) baseline and (c) difference between a and b; -8 deg linear twist, $\mu = 0.3$, 18,300 lbs gross weight.

inboard where the lift is increased due to flap deployment. The drag reductions along the outer rim are larger than the inboard drag increases, and along with the larger moment arm result in a net reduction in rotor torque (and power).

3.3. Analysis, $\mu = 0.35$, 22,000 lbs Gross Weight

Larger power reductions are observed for higher advance ratios and gross weight. At an advance ratio of 0.35 and a high gross weight of 22,000 lbs, a total power reduction of 7.98% was observed (Table 1). The optimal TEF deflections that resulted in this power reduction are shown in Fig. 7. As in the previous case, optimal TEF deflections comprise of a combination of steady, 1/rev and 2/rev deflections components and the deflections are largest on the retreating side.

Figures 8a and 8b show the lift distribution around the rotor disk with optimal TEF deployments and for the baseline rotor, respectively, while Fig. 8c shows the difference between the two. The baseline rotor is even more heavily loaded at the front and rear than the $\mu = 0.3$, 18,300 lbs case (compare Fig. 8b to 5b). From Fig. 8c it is observed that the TEFs again move lift inboard, most notably on the advancing side, while offloading the tips.

Similarly, Figs. 9a and 9b show the drag distribution around the rotor disk with optimal TEF deployments and for the baseline rotor, respectively, while Fig. 9c shows the difference between the two. As with the $\mu = 0.3$, 18,300 lbs case, the baseline rotor drag is highest near the tip in the fourth quadrant, particularly at the rear of the rotor disk (Fig. 9b). The TEFs, by unloading the tips, again reduce the drag along the outer rim and also on the advancing side (Fig. 9c), while the drag increases inboard over most of the rotor disk. These observations are generally true in all cases (combinations of advance ratio and gross weight presented in Table 1), so the power reduction mechanisms discussed are broadly applicable.

Next, the two regions on the rotor disk where the largest drag reductions are observed are examined in further detail. The first region is in the fourth quadrant near the rear of the rotor disk, in the outermost 10% where there are no TEFs present. The second region is on the advancing side where the outermost TEF is deployed. To aid the analysis, the angle of attack distributions for the optimal TEF deployment case, the baseline, and the difference between the two are presented in Figs. 10a, 10b, and 10c, respectively.

For the first region at the rear of the rotor disk, the baseline rotor angle of attack is about 9.5 deg (marked on Fig. 10b). With optimal TEF deployment, the angle of attack in the same region reduces to about 8 deg (marked on Fig. 10a). The Mach number in that region is around 0.5 and the airfoil used is the SC-1095 airfoil. Figures 11a and 11b show the lift and drag coefficients for this airfoil, versus angle of attack, at $M = 0.5$. It can be seen that for the baseline rotor the blade section is close to stall conditions. For the rotor with optimal TEFs working at a lower angle of attack, the blade section produces a very slight reduction in lift (Fig. 11a) but a significant reduction in drag (Fig. 11b). The TEF deployment, then, appears to be reducing drag and power requirement by increasing the stall margin in this region.

For the second region, the Mach number is close to 0.8, and the angle of attack for the baseline rotor is around 1 deg (marked on Fig. 10b). With optimal TEF deploy-

ment, the angle of attack is reduced (to around -0.2 deg, as shown on Fig. 10a). In this region the outermost TEF is deflected to a little over 2 deg (see Fig. 7), and the airfoil is the SC-1094R8 airfoil.

Figure 12 shows the lift and drag coefficients at Mach 0.8 of the baseline SC-1094R8 airfoil and one with a 20% chord TEF deflected 2 deg down, versus angle of attack. Marked on the figure are the operating points for the baseline and rotor and the rotor with optimal TEF deployment. It is observed that with the TEF deployed, the sectional lift coefficient is increased slightly (also reflected in the increase in lift seen in Fig. 8c), while the drag coefficient is reduced (also reflected in the decrease in drag seen in Fig. 9c).

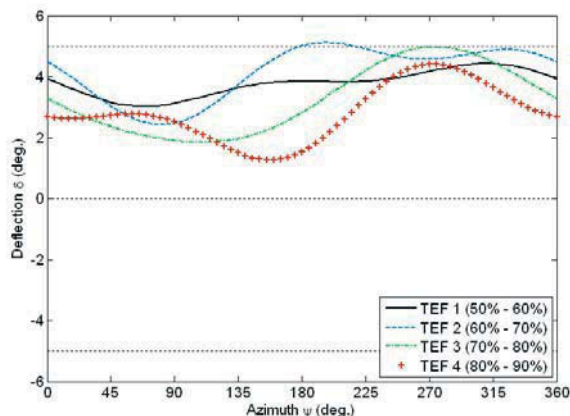


Figure 7. Optimal TEFs deflections; -8 deg linear twist, $\mu = 0.35$, 22,000 lbs gross weight.

3.4. Comparison with UH-60 Non-linear Twist

The previous sections considered a rotor with a -8 deg linear blade twist. Although a linear twist of this magnitude would be fairly representative of a typical rotor, the UH-60 Black Hawk helicopter actually uses a non-linear twist as depicted in Fig. A1 in the Appendix. In this section, optimal TEF deflections and the corresponding power reductions are obtained for the actual Black Hawk nonlinear twist. This is of particular interest since the down-up nonlinear twist changes the aerodynamics at the tip, and the power reductions in the previous section were obtained by offloading the tips. Advance ratios of 0.3, 0.35 and 0.4, and gross weights of 16,000 lbs, 18,300 lbs and 22,000 lbs, are considered in this section.

Table 6 summarizes the power reductions obtained for different conditions. These are presented both in terms of percent power reductions (Table 6a) and actual reductions in horsepower (Table 6b). Power reductions ranging from 2.39% to 5.65% are observed, depending on the flight conditions; with larger reductions observed for high advance ratios and high gross weight. Table 7 summarizes the actual power requirements of the baseline and the optimally flapped rotor for each flight condition. Reductions in profile power and induced power are summarized in Tables 8 and 9, respectively. The same observation as in the linear twist case can be made – the majority of the power reduction comes from reduction in profile power. However, the power reductions obtained on the rotor with nonlinear twist are significantly and consistently lower than those observed on the rotor with -8

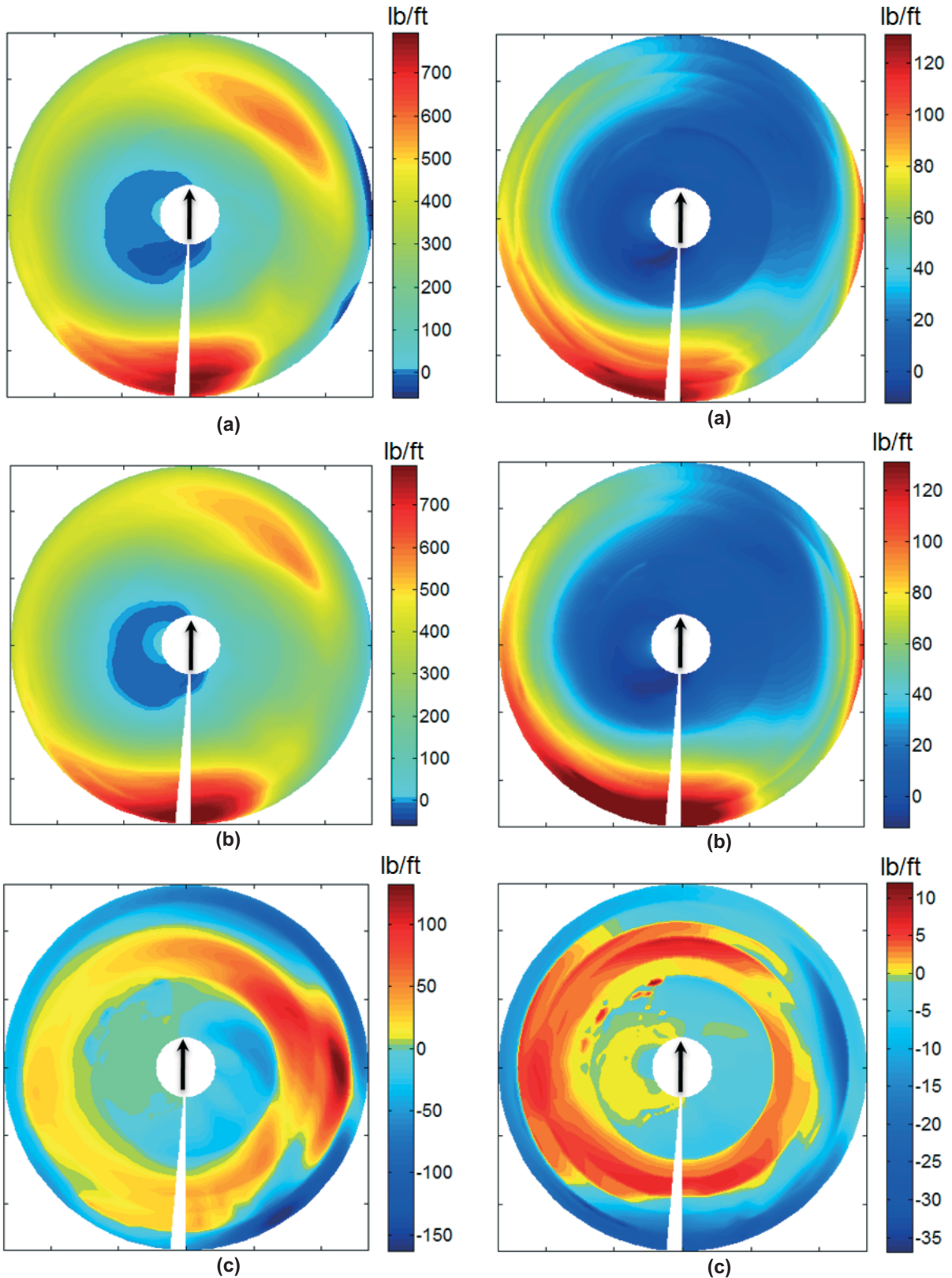
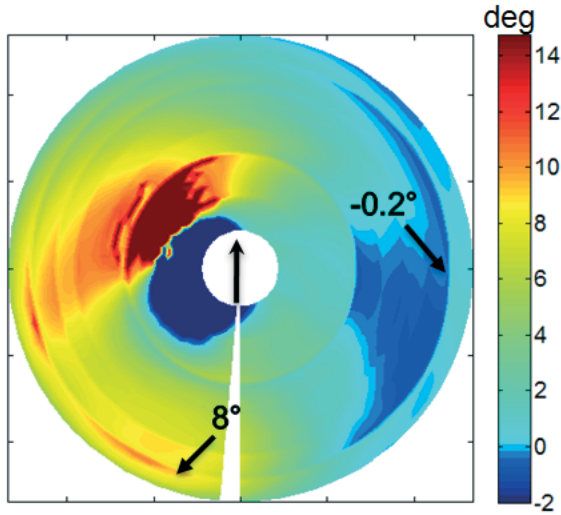
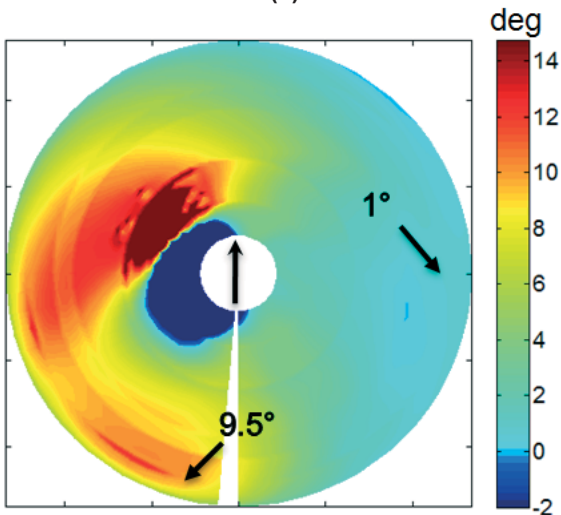


Figure 8. Lift distribution (a) with optimal TEF deployment, (b) baseline, and (c) difference between a and b; -8 deg linear twist, $\mu = 0.35$, 22,000 lbs gross weight.

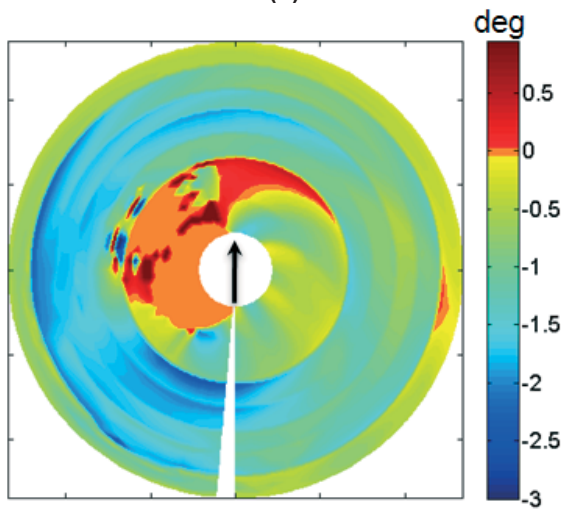
Figure 9. Drag distribution (a) with optimal TEF deployment, (b) baseline, and (c) difference between a and b; -8 deg linear twist, $\mu = 0.35$, 22,000 lbs gross weight.



(a)

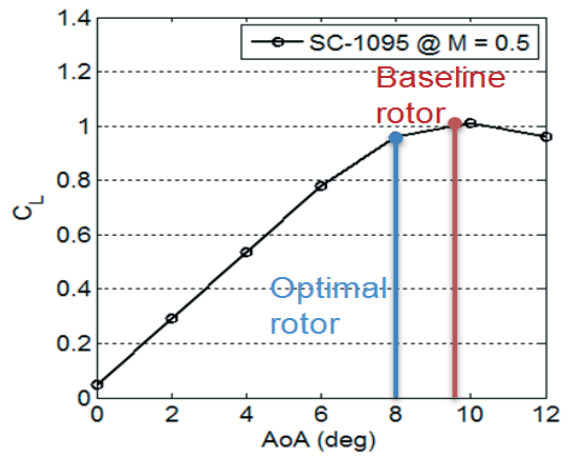


(b)

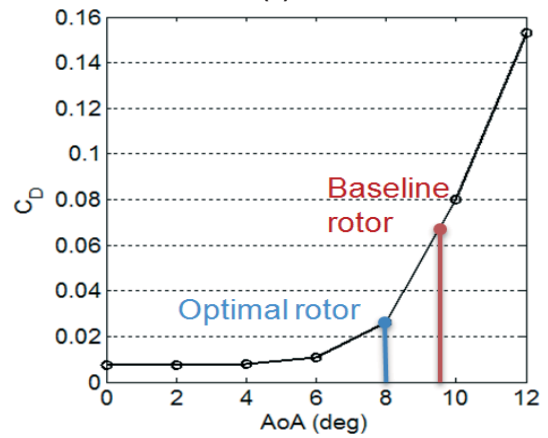


(c)

Figure 10. Angles of attack distribution (a) with optimal TEF deployment, (b) baseline, and (c) difference between a and b; -8 deg linear twist, $\mu = 0.35$, 22,000 lbs gross weight.



(a)



(b)

Figure 11. (a) Lift coefficient and (b) drag coefficient of the SC-1095 airfoil at $M = 0.5$.

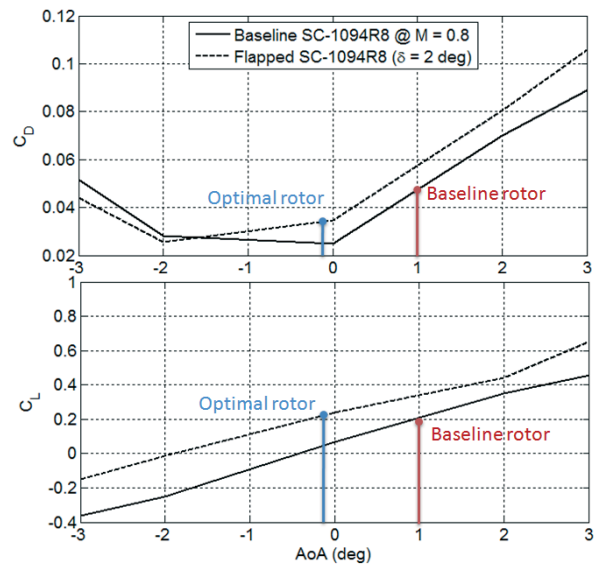


Figure 12. Drag and lift coefficients of baseline SC-1094R8 airfoil and one with 20% chord TEF deflected 2 deg, at $M = 0.8$.

deg linear twist (this is comprehensively presented in Fig. 13). It should be noted that the baseline power requirements for the rotor with nonlinear twist are themselves lower than those for the rotor with -8 deg linear twist (compare Tables 2 and 7). Since the rotor with nonlinear twist is a better starting design, there appears to be less room for improvement.

The $\mu = 0.35$, 22,000 lbs gross weight case is examined in greater detail to facilitate comparison with the rotor with -8 deg linear twist. For the -8 deg linear twist case the baseline rotor power requirement was 2966.83 HP and a 7.98% reduction could be realized with optimal TEF deflection. For the non-linear twist case baseline rotor power was 2779.05 HP and a reduction of 4.19% was realized with optimal TEF deployment shown in Fig. 14. As with the rotor with -8 deg linear twist, the TEF deflections are larger on the retreating side and smaller on the advancing side, but the 2/rev component is less significant in the case of the rotor with nonlinear twist.

Figures 15a and 15b show the lift distribution around the rotor disk with optimal TEF deployments and for the baseline rotor with nonlinear twist, respectively, while Fig. 15c shows the difference between the two. Again the TEFs increase the lift inboard, especially on the advancing side, while offloading the tips. Figures 16a and 16b show the drag distribution around the rotor disk with optimal TEF deployments and for the baseline, respectively, while Fig. 16c shows the difference between the two. For the baseline rotor, the drag is again highest near the rear or the rotor disk out at the blade tip, but not as high for the -8 deg linearly twisted rotor (compare Fig. 16b to Fig. 9b). Drag reductions are observed along the outer rim (Fig. 16c) in the first, third and fourth quadrants of the rotor disk, but the reductions are not as high as seen with the linearly twisted rotor. In the outboard regions in the second quadrant the drag actually increases (unlike the reductions observed for the -8 deg linear twist rotor in Fig. 9c). Again the drag generally increases inboard where the lift is increased due to flap deployment. Additional insight can be gained by examining the lift and drag variation along rotor span at specific azimuthal locations. Figures 17a, 18a and 19a show the lift and drag distributions at 330 deg, 30 deg, and 120 deg azimuth, for the -8 deg linear twist rotor. Similarly, Figs. 17b, 18b, and 19b show the corresponding results for the nonlinear twist case. Results are presented for both the baseline rotor as well as with optimal TEF deflections. A comparison of Figs. 17a and 17b (at 330 deg azimuth) shows the drag reduction at the tip for the -8 deg linearly twisted rotor to be larger than that obtained for the nonlinearly twisted rotor. Also clearly observed on these figures is the lift moving inboard and a corresponding slight increase in inboard drag associated with TEF deployment. A comparison of Figs. 18a and 18b (at 30 deg azimuth) shows the drag of the baseline rotor with nonlinear twist to be lower than that of the baseline rotor with -8 deg linear twist (note the differences in scale), and the drag reductions at the tip with TEF deployment are again smaller. The smaller drag reductions at the rear of the rotor disk is one reason smaller power reductions are observed with TEF actuation on the nonlinearly twisted rotor, compared to the rotor with -8 deg linear twist. The other reason is the drag increase near the blade tips in the second quadrant for the nonlinearly twisted rotor as compared to the drag decrease observed in the case of the rotor with -8 deg linear twist (compare Figs. 16c and 9c). This can be better

Table 6. Total power reduction: (a) percent, and (b) difference in HP, at different advance ratios and gross weights (lbs), non-linear twist.

(a)			
	0.3	0.35	0.4
16,000	2.39	2.67	3.37
18,300	2.83	3.13	3.80
22,000	4.00	4.19	5.65

(b)			
	0.3	0.35	0.4
16,000	40.56	64.36	119.45
18,300	50.95	79.06	139.3
22,000	80.66	116.37	227.05

Table 7. Total power requirement (HP) for baseline and optimal TEF cases, non-linear twist.

		Advance ratio			
		0.3	0.35	0.4	
Gross weight	16,000	1695.19	2409.79	3542.49	Baseline
		1654.63	2345.43	3423.04	Optimal
	18,300	1802.87	2524.41	3667.90	Baseline
		1751.92	2445.35	3528.60	Optimal
	22,000	2015.94	2779.05	4021.58	Baseline
		1935.29	2662.68	3794.53	Optimal

Table 8. Profile power reduction: (a) percent, and (b) difference in HP, at different advance ratios and gross weights (lbs), non-linear twist.

(a)			
	0.3	0.35	0.4
16,000	4.66	6.51	9.21
18,300	4.99	7.65	11.24
22,000	9.38	10.55	16.13

(b)			
	0.3	0.35	0.4
16,000	24.77	44.3	86.24
18,300	27.4	53.77	109.85
22,000	57.41	84.35	194.05

Table 9. Induced power reduction: (a) percent, and (b) difference in HP, at different advance ratios and gross weights (lbs), non-linear twist.

(a)			
	0.3	0.35	0.4
16,000	3.08	3.04	3.63
18,300	4.23	3.42	2.5
22,000	2.67	3.28	1.51

(b)			
	0.3	0.35	0.4
16,000	15.79	20.06	33.22
18,300	23.55	25.29	29.45
22,000	23.55	25.29	29.45

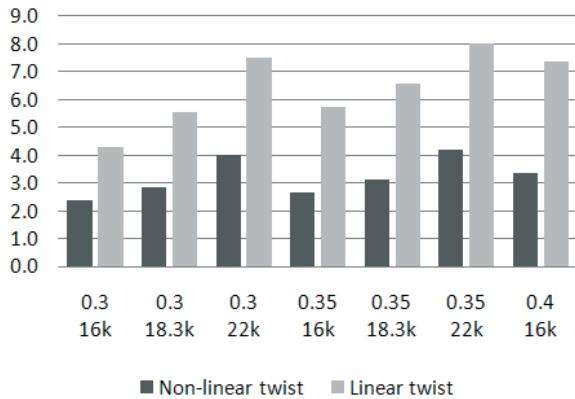


Figure 13. Comparison of percent power reductions for rotor with -8 deg linear twist and non-linear twist.

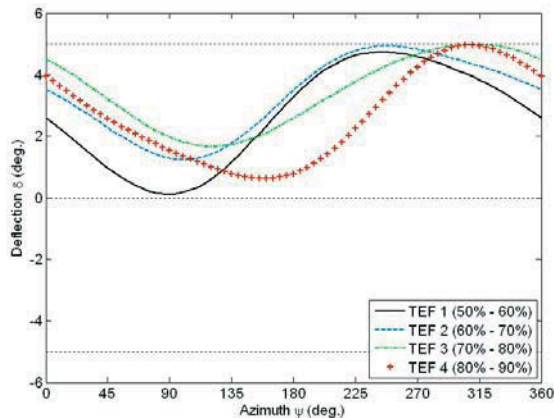


Figure 14. Optimal TEFs deflections; non-linear twist, $\mu = 0.35$, 22,000 lbs gross weight.

understood by examining Figs. 19a and 19b, which show the spanwise lift and drag distributions at 120 deg azimuth for the rotors with -8 deg linear twist and nonlinear twist, respectively. While a strong inboard movement of lift and a good reduction in drag in the outboard region is seen for the rotor with -8 deg linear twist, the lift at the tip is negative for the rotor with nonlinear twist and optimal TEF deflections that minimize power result in this lift becoming more negative. At the high Mach numbers, this results in an increase in drag, which limits the power reduction.

4. CONCLUSIONS

Spanwise-segmented TEFs were examined for rotorcraft power reduction. Four TEFs extending from 50-60%, 60-70%, 70-80% and 80-90% span were considered, and actuated at frequencies of up to 2/rev. A gradient-based optimization scheme was used to determine the optimal deployment of the TEFs that minimized total rotor power, while satisfying vehicle trim. The effect of the TEFs was examined at moderate to very high speeds, and for low through high aircraft gross-weights. The studies were based on a UH-60A type aircraft. In the analysis lift and drag increments associated

with TEF deployment (obtained from CFD computation) were added to airfoil properties of the base SC-1094R8 airfoil. A prescribed wake was used to calculate the inflow around the rotor disk and this allowed for a proper representation of the change in bound and trailed vorticity associated with local changes in lift when a MiTE was deployed.

From the study it was observed that the most significant change in trim parameters associated with deployment of the TEFs was a reduction of rotor collective pitch.

At high gross-weights and advance ratios reductions in rotor power of up to nearly 8% were observed for a -8 deg linear blade twist (is fairly representative of the twist seen on many rotor blades), and up to 5.65% when the nonlinear twist of the UH-60 was considered.

The TEF actuation results in a more optimal airload distribution. In all cases, the tips were offloaded and lift was moved inboard. Although this resulted in a slight increase in drag inboard, the large reduction in drag along the outer rim of the rotor disk and the large moment arm result in a net reduction in rotor torque and power requirement.

The power reduction was predominantly due to a reduction in rotor profile power, especially so at higher gross weights and advance ratios.

The smaller reductions in power for the blade with the nonlinear twist are attributed to a better starting configuration (lower power requirement of the baseline), and the fact that at high speeds and gross weights, the optimal TEF deployment schedule increased the negative lift on the advancing blade tip and consequently the drag in those regions, which partially negated the overall benefits.

REFERENCES

- [1]. Friedmann, P. P., "Rotary Wing Aeroelasticity - Current Status and Future Trends," *AIAA Journal*, Vol. 42, No. 10, Oct. 2004, pp. 1953-1972.
- [2]. McHugh, F. J., and Shaw, J., "Helicopter Vibration Reduction with Higher Harmonic Blade Pitch," *Journal of the American Helicopter Society*, Vol. 23, (4), October 1978, pp. 26-35.
- [3]. Miao, W., Kottapalli, S. B. R., and Frye, H.M., "Flight Demonstration of Higher Harmonic Control (HHC) on S-76," *Proceedings of the 42nd AHS Forum*, Washington D.C., June 2-4, 1986, pp. 777-791.
- [4]. Walsh, D. M., "Flight Test of an Open Loop Higher Harmonic Control System on an S-76A Helicopter," *Proceedings of the 42nd AHS Forum*, Washington D.C., June 2-4, 1986, pp. 831-843.
- [5]. Nguyen, K., and Chopra, I., "Application of Higher Harmonic Control to Rotors Operating at High Speed and Thrust," *Journal of the American Helicopter Society*, Vol. 35, (3), 1990, pp. 78-89.
- [6]. Yen, J. G., "Higher Harmonic Control for Helicopters with Two-Bladed and Four-Bladed Rotors," *Journal of Aircraft*, Vol. 18, No. 12, pp 1064-1069.

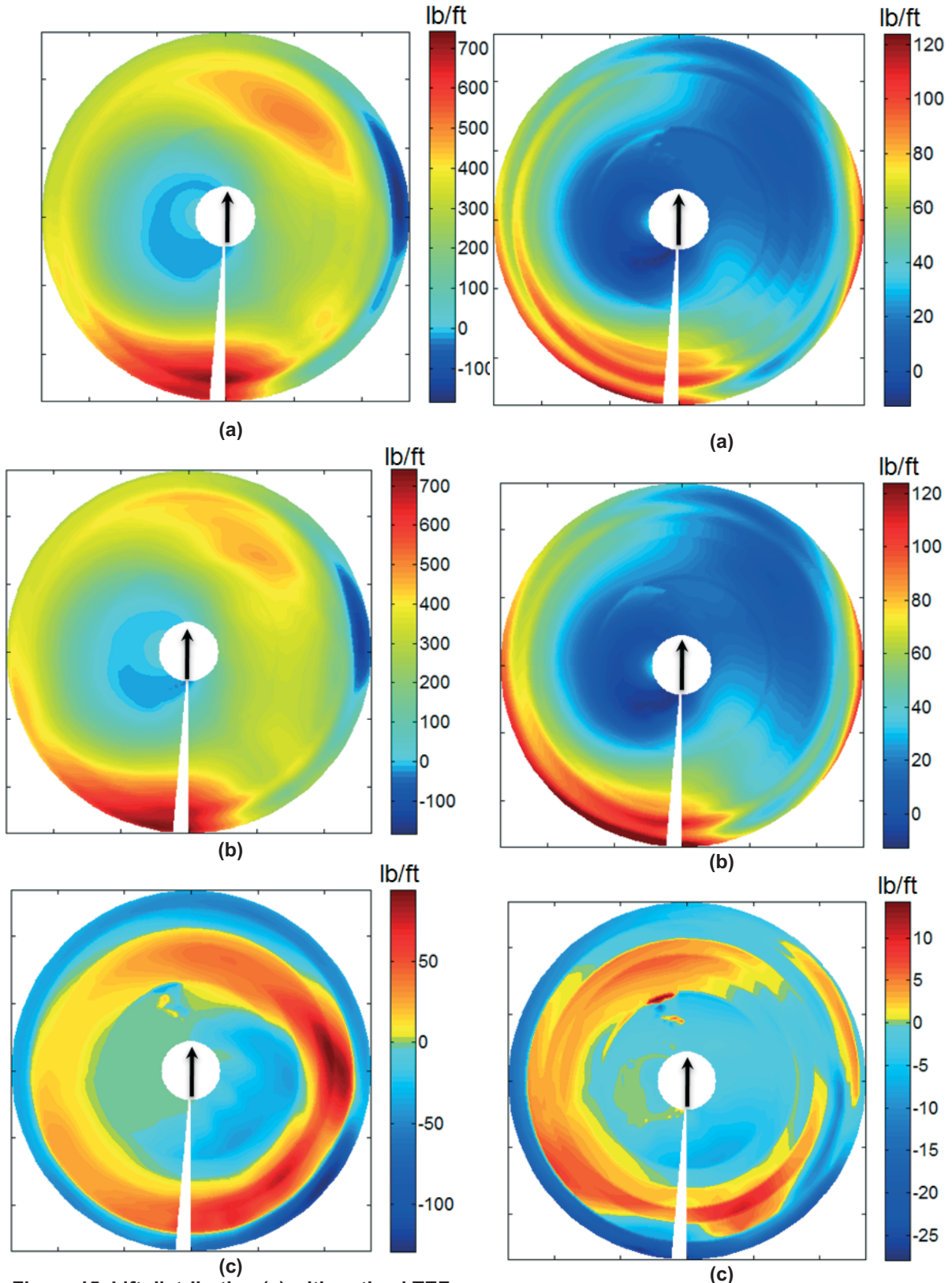


Figure 15. Lift distribution (a) with optimal TEF deployment, (b) baseline, and (c) difference between a and b; non-linear twist, $\mu = 0.35$, 22,000 lbs gross weight.

Figure 16, Drag distribution (a) with optimal TEF deployment, (b) baseline, and (c) difference between a and b; non-linear twist, $\mu = 0.35$, 22,000 lbs gross weight.

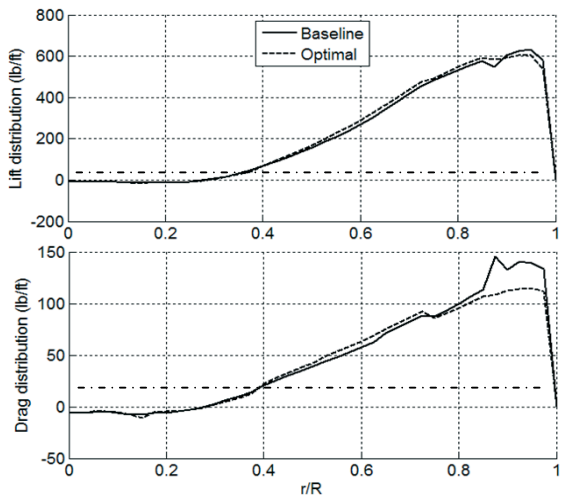


Figure 17a. Spanwise distribution of lift and drag at $\Psi = 330$ deg, -8 deg linear twist.

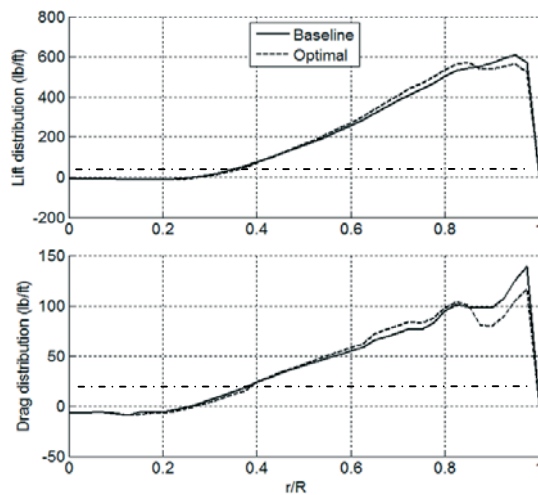


Figure 17b. Spanwise distribution of lift and drag at $\Psi = 330$ deg, non-linear twist.

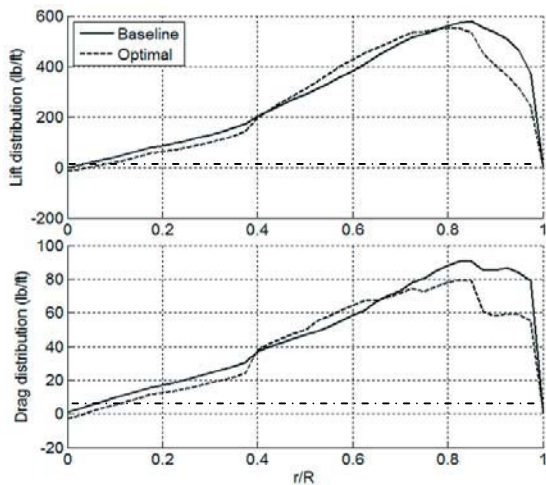


Figure 18a. Spanwise distribution of lift and drag at $\Psi = 30$ deg, -8 deg linear twist.

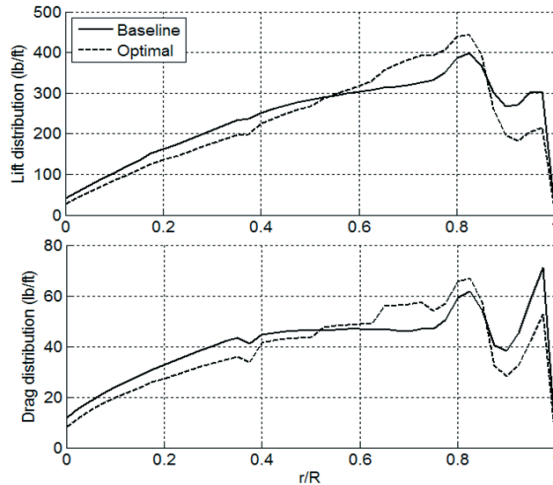


Figure 18b. Spanwise distribution of lift and drag at $\Psi = 30$ deg, non-linear twist.

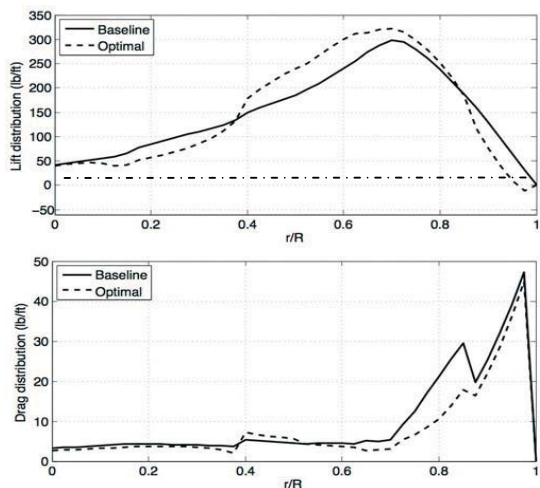


Figure 19a. Spanwise distribution of lift and drag at $\Psi = 120$ deg, -8 deg linear twist.

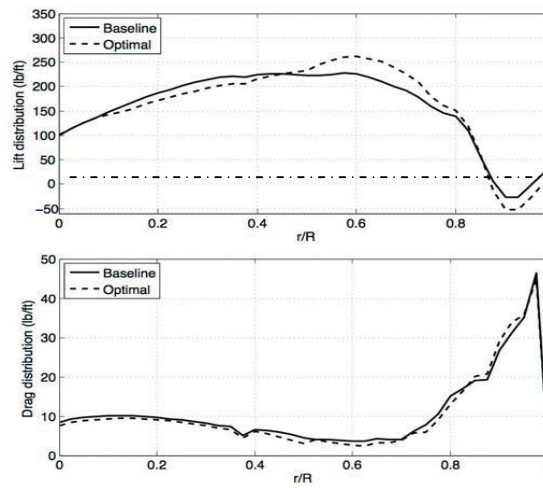


Figure 19b. Spanwise distribution of lift and drag at $\Psi = 120$ deg, non-linear twist.

- [7]. Shaw, J., Albion, N., "Active Control of the Helicopter Rotor for Vibration Reduction", American Helicopter Society 36th Forum, Washington, D.C., May 1980.
- [8]. Robinson, L. H., and Friedmann, P. P., "A Study of Fundamental Issues in Higher Harmonic Control Using Aeroelastic Simulation," *Journal of American Helicopter Society*, Vol. 36, (2), April 1991, pp.32-43.
- [9]. Shaw, J., Albion, N., Hanker, E.J., and Teal, R.S., "Higher Harmonic Control: Wind Tunnel Demonstration of Fully Effective Vibratory Hub Force Suppression," *Journal of the American Helicopter Society*, Vol. 34, (1), January 1989, pp. 14-25..
- [10]. Nguyen, K., and Chopra, I., "Effects of Higher Harmonic Control on Rotor Performance and Control Loads," *Journal of Aircraft*, Vol. 29, No. 3, May-June 1992, pp. 336-342.
- [11]. Jacklin, S. A., and Nguyen, K., Blaas, A., and Richter, P., "Full-Scale Wind Tunnel test of a Helicopter Individual Blade Control System," *Proceedings of the American Helicopter Society 50th Annual Forum*, Washington, DC, May 1994, pp. 579-596.
- [12]. Jacklin, S.A., Nguyen, K., Richter, P., and Blaas, A., "Reduction in Helicopter BVI Noise, Vibration, and Power Consumption through Individual Blade Control," *Proceedings of the American Helicopter Society 51th Annual Forum*, FortWorth, TX, May 1995.
- [13]. Cheng, R. P., Theodore, C. R., and Celi, R., "Effects of Two/rev Higher Harmonic Control on Rotor Performance," *Journal of the American Helicopter Society*, Vol. 48, No. 1, Jan. 2003, pp.18-27.
- [14]. Cheng, R. P., and Celi, R., "Optimum Two-Per-Revolution Inputs for Improved Rotor Performance," *Journal of Aircraft*, Vol. 42, No. 6, Nov-Dec 2005, pp. 1409-1417.
- [15]. Kessler, C., Fuerst, D., Arnoold, U. T. P., "Open Loop Flight Test Results and Closed Loop Status of the IBC System on the CH-53G Helicopter," *Proceedings of the AHS 59th Annual Forum*, Phoenix, AZ, May 2003.
- [16]. Arnold, U. T. P., "Recent IBC Flight Test Results from the CH-53G Helicopter," *Proceedings of the 29th European Rotorcraft Forum*, Friedrichshafen, Germany, September 2003.
- [17]. Liu, L., Freidmann, P. P., Kim, I., and Bernstein, D., "Rotor Performance Enhancement and Vibration Reduction in Presence of Dynamic Stall Using Actively Controlled Flaps," *Journal of the American Helicopter Society*, Vol. 53, (4), October 2008, pp. 338-350.
- [18]. Yeo. H., "Assessment of Active Controls for Rotor Performance Enhancement," *Journal of the American Helicopter Society*, Vol. 53, (2), April 2008, pp. 152-163.
- [19]. Moffitt, R. C., Bissell, J. R., "Theory and Application of Optimum Airloads to Rotor in Hover and Forward Flight," American Helicopter Society 38th Annual Forum, 1982.
- [20]. Hall, S. R., Yang, K. Y., Hall, K. C., "Helicopter Rotor Lift Distributions for Minimum-Induced Power Loss," *Journal of Aircraft*, Vol. 31, No. 4, July-Aug. 1994.
- [21]. Rand, O., Khromov, V., Peyran, R. J., "Minimum-Induced Power Loss of a Helicopter Rotor via Circulation Optimization," *Journal of Aircraft*, Vol. 41, No. 1, 2004.
- [22]. Bae, E.-S., Gandhi, F., Maughmer, M., "Optimally Scheduled Deployment of Gurney Flaps for Rotorcraft Power Reduction," *Proceedings of the 65th Annual Forum of the American Helicopter Society*, Grapevine, Texas, May 27-29, 2009.
- [23]. Léon' O., Hayden, E., and Gandhi, F., "Rotorcraft Operating Envelope Expansion Using Extendable Chord Sections," *Proceedings of the 65th Annual Forum of the American Helicopter Society*, Grapevine, Texas, May 27-29, 2009.
- [24]. Steiner, J., Gandhi, F., Yoshizaki, Y., "An Investigation of Variable Rotor RPM on Performance and Trim," *Proceedings of the 64th Annual Forum of the American Helicopter Society*, Montreal, Canada, April 29 – May 1, 2008
- [25]. Bluman, J., Gandhi, F., "Reducing Trailing Edge Flap Deflection Requirements in Swashplateless Primary Control with a Moveable Horizontal Tail," *Proceedings of the 65th Annual Forum of the American Helicopter Society*, Grapevine, Texas, May 27-29, 2009.
- [26]. Duling, C. T., "Further Investigations on Helicopter Primary Control Using Trailing Edge Flaps," Master's Thesis, the Pennsylvania State University, University Park, May 2009.
- [27]. Duling, C. T., Gandhi, F., Baeder, J., Jose, A. I., "Analysis of CFD Predictions for the SC-1094R8 Airfoil with a Trailing Edge Flap," Submitted to the *Journal of Aircraft*, March 2009.
- [28]. Bousman, W.G., "Aerodynamic Characteristics of SC1095 and SC1094R8 Airfoils," NASA/TP-2003-212265, 2003, pp. 26-37.

APPENDIX

Table A1. Key UH-60A Helicopter Properties.

Parameter	Symbol	Value
Rotor Radius	R	26.83 ft
Angular Velocity	Ω	27 rd/s
Blade Root Cutout	R_{co}	3.83 ft
Blade Chord [†]	c	1.73 ft
Blade Twist	θ_{tw}	-16°
Blade Solidity	σ	.0822
Flapping moment of inertia	I_{β}	1618 slug.ft ²
Rotor Blade Airfoil [†]		SC-1095
		SC-1094R8
Shaft Forward Tilt	α_{Sx}	3°
Tail Rotor Cant Angle	Φ_{TR}	20°
Longitudinal CG Offset [†]	x_{cg}	1.525 ft
Lateral CG Offset [†]	y_{cg}	0 ft
Vertical CG Offset [†]	z_{cg}	-5.825 ft
Lon. Stabilator offset [†]	x_{ht}	29.925 ft
Lat. Stabilator offset [†]	y_{ht}	0 ft
Vert. Stabilator offset [†]	z_{ht}	-5.915 ft
Lon. Tail Rotor offset [†]	x_{tr}	32.565 ft
Lat. Tail Rotor offset [†]	y_{tr}	0 ft
Vert. Tail Rotor offset [†]	z_{tr}	0.805 ft

[†]Varies span-wise

[†] Distance wrt the hub

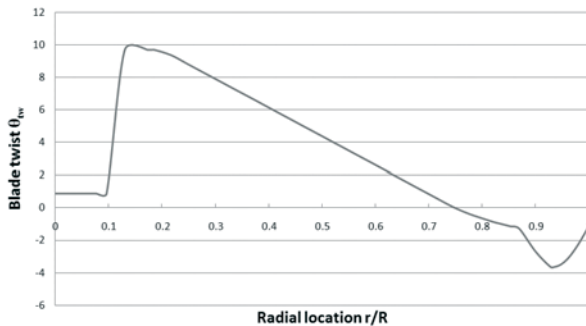


Figure A1. UH-60 non-linear blade twist.

Table A2. TEF optimal controls for -8 deg linear twist rotor.

GW	μ	δ_0	δ_{1c}	δ_{1s}	δ_{2c}	δ_{2s}	
16,000 lbs	0.3	3.350	-0.068	-1.359	1.094	0.103	TEF1
		3.212	0.264	-1.336	0.705	0.327	TEF2
		2.923	0.801	-1.549	0.752	0.541	TEF3
		2.199	0.855	-1.063	-0.343	0.534	TEF4
	0.35	3.752	0.239	-0.779	0.654	0.327	TEF1
		3.698	0.654	-1.092	0.589	0.058	TEF2
		3.267	0.926	-1.521	-0.100	0.736	TEF3
		2.597	1.381	-1.427	-0.686	0.147	TEF4
	0.4	3.036	0.982	0.805	0.852	0.132	TEF1
		3.106	1.505	0.319	0.498	-0.109	TEF2
		3.106	1.626	-0.641	-0.824	-0.058	TEF3
		2.788	0.961	-0.875	-1.092	-0.384	TEF4
18,300 lbs	0.3	3.750	-0.263	-1.037	0.702	-0.186	TEF1
		3.490	0.513	-0.854	0.565	0.055	TEF2
		3.596	0.585	-1.571	0.811	0.602	TEF3
		2.856	1.041	-1.244	-0.313	0.629	TEF4
	0.35	4.038	0.059	-0.725	0.671	0.033	TEF1
		3.893	0.140	-1.188	0.413	0.168	TEF2
		3.415	0.633	-1.390	0.325	0.316	TEF3
		2.665	1.165	-1.380	-0.705	-0.134	TEF4
	0.4	4.105	-0.347	-0.785	0.535	-0.447	TEF1
		4.106	-0.115	-1.060	0.406	-0.241	TEF2
		3.472	0.388	-1.406	0.246	0.201	TEF3
		3.041	1.058	-0.926	-0.402	0.439	TEF4
22,000 lbs	0.3	3.671	-0.027	-0.747	-0.100	-0.414	TEF1
		4.139	-0.178	-1.269	0.453	-0.198	TEF2
		3.186	0.174	-1.602	-0.185	-0.065	TEF3
		2.669	0.507	-1.078	-0.906	0.036	TEF4

Table A3. TEF optimal controls for the non-linear twist rotor.

GW	μ	δ_0	δ_{1c}	δ_{1s}	δ_{2c}	δ_{2s}	
16,000 lbs	0.3	1.780	0.881	-3.384	1.572	0.075	TEF1
		2.410	0.905	-3.143	1.157	0.594	TEF2
		2.687	1.581	-2.037	0.368	0.356	TEF3
		1.840	1.980	-1.483	-0.206	-0.184	TEF4
	0.35	2.771	0.765	-2.626	0.658	0.167	TEF1
		3.025	1.596	-2.159	0.378	0.894	TEF2
		2.655	2.199	-1.844	0.114	0.760	TEF3
		1.736	2.488	-1.125	0.287	-0.405	TEF4
	0.4	2.836	1.155	-1.938	0.651	0.126	TEF1
		3.127	1.299	-1.407	0.445	0.232	TEF2
		2.904	1.742	-1.396	0.233	0.267	TEF3
		2.242	2.227	-0.944	0.112	-0.356	TEF4
18,300 lbs	0.3	0.937	0.323	-2.485	1.285	-1.239	TEF1
		2.311	0.399	-2.631	1.078	-0.095	TEF2
		2.677	1.032	-1.821	0.150	-0.052	TEF3
		1.757	1.673	-1.379	-0.954	-0.461	TEF4
	0.35	2.500	0.615	-3.037	0.921	0.289	TEF1
		3.474	0.976	-2.056	0.569	0.601	TEF2
		2.926	1.587	-1.794	0.264	0.222	TEF3
		2.325	2.069	-1.176	-0.121	-0.483	TEF4
	0.4	3.839	-0.105	-1.084	1.027	-0.128	TEF1
		3.888	0.741	-1.398	0.334	0.399	TEF2
		3.292	1.904	-1.384	-0.203	0.609	TEF3
		2.465	2.423	-0.819	-0.114	-0.152	TEF4
22,000 lbs	0.3	2.567	0.404	-1.876	0.167	0.172	TEF1
		3.352	0.968	-1.707	0.497	0.353	TEF2
		3.178	1.588	-1.224	0.111	0.372	TEF3
		2.888	1.975	-1.289	-0.006	0.295	TEF4
	0.35	2.612	-0.432	-2.244	0.287	0.189	TEF1
		3.253	-0.077	-1.813	0.148	0.176	TEF2
		3.404	0.939	-1.317	0.098	0.105	TEF3
		2.632	1.609	-1.379	-0.294	-0.221	TEF4
	0.4	4.123	0.154	-0.842	0.050	-0.012	TEF1
		4.257	0.523	-0.512	0.046	-0.006	TEF2
		3.186	0.893	-1.596	-0.004	0.016	TEF3
		2.925	1.902	-1.112	-0.058	-0.004	TEF4